

Photoluminescence spectra of n -doped double quantum wells in a parallel magnetic field

Danhong Huang

Air Force Research Laboratory (AFRL/VSSS), Kirtland Air Force Base, New Mexico 87117

S. K. Lyo

Sandia National Laboratories, Albuquerque, New Mexico 87185

(Received 27 July 1998; revised manuscript received 29 September 1998)

We show that the photoluminescence (PL) line shapes from tunnel-split ground sublevels of n -doped thin double quantum wells (DQW's) are sensitively modulated by an in-plane magnetic field B_{\parallel} at low temperatures (T). The modulation is caused by the B_{\parallel} -induced distortion of the electronic structure. The latter arises from the relative shift of the energy-dispersion parabolas of the two quantum wells (QW's) in \vec{k} space, both in the conduction and valence bands, and formation of an anticrossing gap in the conduction band. Using a self-consistent density-functional theory, the PL spectra and the band-gap narrowing are calculated as a function of B_{\parallel} , T , and the homogeneous linewidths. The PL spectra from symmetric and asymmetric DQW's are found to show strikingly different behavior. In symmetric DQW's with a high density of electrons, two PL peaks are obtained at $B_{\parallel}=0$, representing the interband transitions between the pair of the upper (i.e., antisymmetric) levels and that of the lower (i.e., symmetric) levels of the ground doublets. As B_{\parallel} increases, the upper PL peak develops an \mathcal{N} -type kink, namely a maximum followed by a minimum, and merges with the lower peak, which rises monotonically as a function of B_{\parallel} due to the diamagnetic energy. When the electron density is low, however, only a single PL peak, arising from the transitions between the lower levels, is obtained. In asymmetric DQW's, the PL spectra show mainly one dominant peak at all B_{\parallel} 's. In this case, the holes are localized in one of the QW's at low T and recombine only with the electrons in the same QW. At high electron densities, the upper PL peak shows an \mathcal{N} -type kink like in symmetric DQW's. However, the lower peak is absent at low B_{\parallel} 's because it arises from the inter-QW transitions. Reasonable agreement is obtained with recent data from GaAs/Al_{0.3}Ga_{0.7}As DQW's. [S0163-1829(99)00411-7]

I. INTRODUCTION

Physical phenomena in tunnel-coupled quasi-two-dimensional double quantum well (DQW) structures have received increasing attention recently. These systems show novel electronic and transport properties, which are absent in single QW's. Although the effect of the Landau quantization in perpendicular magnetic fields in the growth (i.e., z direction) has been examined extensively in the past, interesting effects due to purely in-plane magnetic fields ($B_{\parallel} \parallel x$) began to be discovered only recently.¹⁻¹⁴ In weakly coupled DQW's with a wide center barrier, tunneling conductance can be tuned by B_{\parallel} .¹⁻⁴ In strongly coupled DQW's with a thin center barrier, B_{\parallel} introduces anticrossing in the energy dispersion curves,⁵ yielding modulations in the transport properties such as the resistance⁵⁻¹¹ and the cyclotron mass.¹¹⁻¹⁴ In this paper, we calculate the photoluminescence (PL) line shapes from tunnel-split ground-sublevel doublets of strongly coupled n -doped DQW's and show that the line shapes are sensitively modulated by B_{\parallel} at low temperatures (T). Our theoretical results yield strikingly different B_{\parallel} -dependent behavior of the PL spectra for symmetric and asymmetric DQW's. The PL line shapes, evaluated for GaAs/Al _{η} Ga_{1- η} As DQW's with $\eta=0.3$, agree with recent data.

The effect of B_{\parallel} is to displace the origins of the transverse crystal momenta k_y in the two QW's away from each other in \vec{k} space by $\Delta k_y = d/\ell_{\parallel}^2$, where d is the center-to-center

distance between the QW's and $\ell_{\parallel} = \sqrt{\hbar c/eB_{\parallel}}$ is the magnetic length. Carrier motion in the k_x direction is undisturbed. As a result, the energy-dispersion parabolas of the two QW's, in the effective mass approximation, intersect each other. The degeneracy at the crossing is removed due to tunneling, thereby yielding an energy gap in the k_y direction as illustrated in Fig. 1 for symmetric DQW's and in Fig. 2 for asymmetric DQW's. The lower edge of the gap becomes

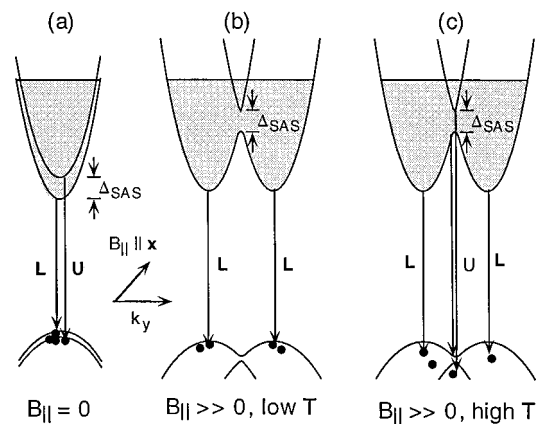


FIG. 1. PL energies (shown by vertical arrows) in n -doped symmetric DQW's (a) at $B_{\parallel}=0$, (b) in high B_{\parallel} 's and low temperatures, and (c) in high B_{\parallel} 's and high temperatures. The quantity Δ_{SAS} indicates energy splitting between the symmetric and antisymmetric ground sublevels. The splittings for the holes are negligibly small.

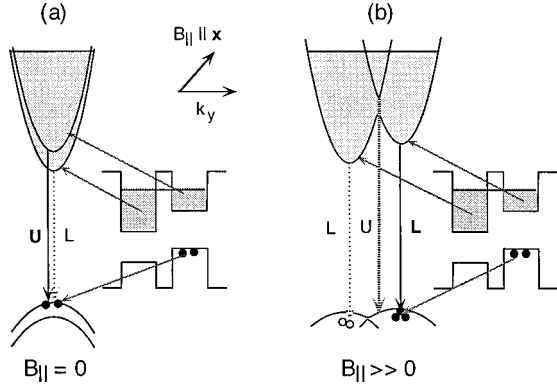


FIG. 2. PL energies (shown by vertical arrows) in n -doped asymmetric DQW's (a) at $B_{\parallel} = 0$ and (b) in high B_{\parallel} 's. The energy splitting in (a) is mainly due to the energy mismatch between the bottoms of the QW's. The holes in (b) are localized in the right QW at low temperatures as shown by the black dots and become delocalized at high temperatures as illustrated by the empty dots.

a saddle point at a sufficiently high B_{\parallel} as shown in Figs. 1(b), 1(c), and 2(b), with a logarithmic singularity in the density of states. With increasing B_{\parallel} , the two paraboloids move farther away from each other, passing the anticrossing gap through the chemical potential μ indicated by the horizontal lines in Fig. 1.¹⁰⁻¹² The bottoms of the parabolas rise in energy with B_{\parallel} due to the diamagnetic energy. The holes here are heavy holes (i.e., $|3/2, \pm 3/2\rangle$). Light holes have larger confinement energy and are not populated at low T .

Qualitative understanding of the key features of the B_{\parallel} -dependent PL between the majority electrons and the photogenerated holes in the ground doublets can be gained from inspection of the in-plane energy-dispersion curves and the momentum-conserving interband transitions illustrated by the vertical arrows in Figs. 1 and 2 for symmetric and asymmetric DQW's, respectively. In symmetric DQW's at $B_{\parallel} = 0$, the interband transitions between the ground levels (i.e., lower branches) and the excited levels (i.e., upper branches) yield two PL peaks separated by the gap energy Δ_{SAS} . The doublet splitting of the hole energy is negligibly small due to the large confinement mass of the heavy holes. The saddle point is formed at $k_y = 0$ above a sufficiently high B_{\parallel} (~ 4 T in our example) in the conduction band due to strong tunnel-induced repulsion between the upper and lower branches. At this field, the minima of the electron energy move away from $k_y = 0$ abruptly as shown in Fig. 1(b). On the other hand, the repulsion between the lower and upper branches is weak in the valence band. The hole energy minima move away from $k_y = 0$ continuously as B_{\parallel} increases, depopulating the holes from the $k_y = 0$ area at low temperatures and reducing the PL intensity from the upper peak. As a result, the upper PL peak energy as a function of B_{\parallel} shows an \mathcal{N} -type kink, namely a maximum followed by a minimum, and merges with the lower peak at higher B_{\parallel} 's as observed recently.¹⁵ The maximum arises from the initial rise due to the diamagnetic energy. At high temperatures, however, the holes still populate the area near the anticrossing gap at $k_y = 0$ even at high B_{\parallel} 's, yielding three (two) PL peaks when the chemical potential is above (inside) the gap at high (low) doping densities. This behavior is illustrated in Fig. 1(c).

In asymmetric DQW's, on the other hand, holes are localized in one of the QW's at low temperatures as shown in Fig. 2. Electron-hole recombinations then occur mainly in the QW where the holes reside, yielding a single PL peak at all B_{\parallel} 's as illustrated in Fig. 2 and observed recently.¹⁵ At high temperatures, however, more PL peaks can occur as illustrated by broken arrows in Fig. 2(b) due to thermal excitations of the holes.

The organization of this paper is as follows. In the next section, we present a self-consistent density-functional theory for the eigen energies and eigen states. A formalism for the PL line shape is given in Sec. III. Numerical results and discussions are presented in Sec. IV for the B_{\parallel} -, T -, and Γ -dependent behavior of the PL line shapes of symmetric and asymmetric DQW's, and for the band-gap narrowing.^{16,17} The paper is concluded in Sec. V with some brief remarks.

II. EIGEN-ENERGIES AND FUNCTIONS FOR ELECTRONS AND HOLES

Let us consider a double quantum well (DQW) structure in which the width of both quantum wells is L_W . These two quantum wells (QW's) are separated by a center barrier with thickness L_B . Both the left and right QW's are modulation δ doped with the sheet densities N_D^L and N_D^R at the left and right sides of DQW outer edges. The thickness of the spacer layer between δ -doping layer and the outer edges of the DQW's is L_S . The well material is GaAs and the barrier material is $\text{Al}_{\eta}\text{Ga}_{1-\eta}\text{As}$ with $\eta = 0.30$ being the alloy composition. An external magnetic field \mathbf{B}_{\parallel} is applied in the x direction parallel to the planes of the QW's. In this paper, we will study both symmetric and asymmetric DQW's. For asymmetric DQW's, either the widths of two quantum wells are not identical or the δ -doping densities on the left and right are not the same.

It is well known that the ground state of electron and hole gases in quantum wells can be accurately calculated by the Kohn-Sham density-functional theory at low temperatures. In this paper, we calculate the PL spectrum from the tunnel-split ground states of electrons and heavy-holes. The eigen function $\phi_{j,k_y}^e(z)$ and energy $E_j^e(k_y)$ for electrons in the Landau gauge can be calculated from the Kohn-Sham density-functional theory

$$\begin{aligned} & \left[-\frac{\hbar^2}{2} \frac{d}{dz} \left(\frac{1}{m_e^*(z)} \frac{d}{dz} \right) + V_{DQW}^c(z) + \frac{\hbar^2}{2m_e^*(z)} \left(k_y - \frac{z}{\ell_{\parallel}^2} \right)^2 \right] \\ & \times \phi_{j,k_y}^e(z) + \{V_H^e(z) + V_{XC}^e[n_e(z)]\} \phi_{j,k_y}^e(z) \\ & = E_j^e(k_y) \phi_{j,k_y}^e(z). \end{aligned} \quad (1)$$

In Eq. (1), $m_e^*(z)$ is the position-dependent confinement mass of the electrons in the z direction, which equals $0.0665 m_0$ inside the GaAs wells and $(0.0665 + 0.083\eta) m_0$ in the $\text{Al}_{\eta}\text{Ga}_{1-\eta}\text{As}$ barriers, and m_0 is the free-electron mass, j is the sublevel index, and $V_{DQW}^c(z) = 0.57 \times 1.427\eta$ (eV) is the conduction-band offset. The total electron energy is

$$E_j^e(\mathbf{k}_{\parallel}) = E_j^e(k_y) + \frac{\hbar^2 k_x^2}{2m_j^e(k_y)}, \quad (2)$$

where k_x is the electron wave vector in the x direction. The in-plane effective mass of electrons $m_j^e(k_y)$ in the j th sub-level is given by

$$\frac{1}{m_j^e(k_y)} = \frac{P_j^e(k_y)}{m_W^e} + \frac{1 - P_j^e(k_y)}{m_B^e}. \quad (3)$$

Here, the dwelling probability for the electrons in the DQW region is

$$P_j^e(k_y) = \int_{DQW \text{ Region}} [\phi_{j,k_y}^e(z)]^2 dz, \quad (4)$$

and $m_W^e = 0.0665m_0$, $m_B^e = (0.0665 + 0.083\eta)m_0$ are the in-plane effective masses of the electrons in the QW and barriers, respectively. The Hartree potential $V_H^e(z)$ for the electrons is determined from Poisson's equation

$$\frac{d}{dz} \left[\epsilon_b(z) \frac{d}{dz} V_H^e(z) \right] = \frac{e^2}{\epsilon_0} \sum_{\alpha=L,R} N_D^\alpha \delta(z - z_\alpha) - n_e(z), \quad (5)$$

and the exchange-correlation potential $V_{XC}^e[n_e(z)]$ for the electrons in the local-density approximation¹⁸ is given by

$$V_{XC}^e[n_e(z)] = - \frac{e^2}{8\pi\epsilon_0\epsilon_b(z)a_0^*(z)} \left\{ 1 + 0.0545r_s(z) \times \ln \left[1 + \frac{11.4}{r_s(z)} \right] \right\} \left[\frac{2}{\pi(4/9\pi)^{1/3}r_s(z)} \right]. \quad (6)$$

In Eq. (5), z_α (with $\alpha=L,R$) is the δ -doping layer position. In Eq. (6),

$$a_0^*(z) = \frac{4\pi\epsilon_0\epsilon_b(z)\hbar^2}{m_e^*(z)e^2} \quad (7)$$

is the effective Bohr radius and

$$r_s(z) = \left\{ \frac{4}{3} \pi [a_0^*(z)]^3 n_e(z) \right\}^{-1/3} \quad (8)$$

is the dimensionless electron density parameter. Here, $\epsilon_b(z)$ is the dielectric constant that equals 12.04 in the QW's and (12.04–2.93 η) in the barriers, respectively. The electron density function is calculated from

$$n_e(z) = \frac{2}{A} \sum_{j,\mathbf{k}_{\parallel}} [\phi_{j,k_y}^e(z)]^2 f_0^e[E_j^e(\mathbf{k}_{\parallel})], \quad (9)$$

where A is the sample cross-section area. The Fermi-Dirac distribution function $f_0^e[E_j^e(\mathbf{k}_{\parallel})]$ for electrons in the equilibrium state is

$$f_0^e[E_j^e(\mathbf{k}_{\parallel})] = \left[\exp \left(\frac{E_j^e(\mathbf{k}_{\parallel}) - \mu_e}{k_B T} \right) + 1 \right]^{-1}, \quad (10)$$

and the electron chemical potential μ_e is determined by the charge neutral condition

$$N_D^L + N_D^R = \int_{-\infty}^{+\infty} n_e(z) dz = \frac{2}{A} \sum_{j,\mathbf{k}_{\parallel}} f_0^e[E_j^e(\mathbf{k}_{\parallel})]. \quad (11)$$

Here, the small photo-excited electron-hole density is assumed to be negligibly small and the semiconductor surfaces are assumed to be far away.

In III-V semiconductors, such as GaAs and $\text{Al}_x\text{Ga}_{1-x}\text{As}$, mixing between the electrons and holes is extremely small due to the large energy band gap. However, there still exists mixing between the heavy and light hole states, which creates nonparabolic energy dispersions of heavy and light holes.^{19–21} It is well known that these nonparabolic energy dispersions are only important for the hole states with large in-plane momentum. Here, the density of photo-excited holes is so low that only the hole states with very small in-plane momentum at low temperatures are occupied. As a result, mixing of the heavy- and light-hole states can be neglected in our calculation. The eigen function $\phi_{j,k_y}^h(z)$ and energy $E_j^h(k_y)$ for the holes can be determined from the following Schrödinger equation in the Landau gauge

$$\left[-\frac{\hbar^2}{2} \frac{d}{dz} \left(\frac{1}{m_h^*(z)} \frac{d}{dz} \right) + V_{DQW}^p(z) + \frac{\hbar^2}{2m_h^*(z)} \left(k_y - \frac{z}{\ell_{\parallel}^2} \right)^2 \right] \times \phi_{j,k_y}^h(z) + \{V_H^h(z) + V_C^h[n_e(z)]\} \phi_{j,k_y}^h(z) = E_j^h(k_y) \phi_{j,k_y}^h(z), \quad (12)$$

where $m_h^*(z)$ is the confinement mass of the holes in the z direction and equals 0.4535 in the QW's and (0.4535 + 0.14 η) in the barriers. In Eq. (12), $V_{DQW}^p(z) = 0.43 \times 1.427\eta$ (eV) is the valence-band offset. The Hartree potential for the holes is $V_H^h(z) = -V_H^e(z)$, and the correlation energy is¹⁸

$$V_C^h[n_e(z)] = - \frac{e^2}{8\pi\epsilon_0\epsilon_b(z)a_0^*(z)} \left[\frac{3}{4} + 0.6213u_s(z) \times \left\{ (1 + u_s(z)^3) \ln \left(1 + \frac{1}{u_s(z)} \right) + \frac{u_s(z)}{2} - u_s(z)^2 - \frac{1}{3} \right\} \right] \times \left[\frac{2}{11.4\pi(4/9\pi)^{1/3}u_s(z)} \right], \quad (13)$$

where $u_s(z) = r_s(z)/11.4$. The total hole energy is

$$E_j^h(\mathbf{k}_{\parallel}) = E_j^h(k_y) + \frac{\hbar^2 k_x^2}{2m_j^h(k_y)}, \quad (14)$$

where the effective mass of holes $m_j^h(k_y)$ in the j th sublevel is given by

$$\frac{1}{m_j^h(k_y)} = \frac{P_j^h(k_y)}{m_W^h} + \frac{1 - P_j^h(k_y)}{m_B^h}. \quad (15)$$

Here, the dwelling probability for the holes in the DQW region is

$$P_j^h(k_y) = \int_{DQW \text{ Region}} [\phi_{j,k_y}^h(z)]^2 dz, \quad (16)$$

and $m_W^h = 0.09$, $m_B^h = (0.09 + 0.10\eta)$ are the in-plane effective masses of holes in the QW's and barriers, respectively. The effective masses and the band offsets are summarized in Table I.

III. PHOTOLUMINESCENCE SPECTRA

The PL spectrum is determined by the following spontaneous emission rate:^{22,23}

$$\begin{aligned} R_{sp}(\omega) &= \frac{\sqrt{\epsilon_b} \omega e^2}{\pi^3 \hbar m_0 \epsilon_0 c^3 L_z} \int_{E_1^e(k_y^{min})}^{\hbar\omega - E_g - E_1^e(k_y^{min})} dE' f_0^e(\hbar\omega - E_g - E') f_0^h(E') \\ &\times \frac{2}{A} \sum_{j,j';\mathbf{k}_\parallel} S[\hbar\omega - E_g - E_j^e(k_y^{min}) - E_{j'}^h(k_y^{min})] \left[\frac{|M_{j,j'}^{e,h}(k_y)|^2}{m_0} \right] \\ &\times \frac{\Gamma_e \Gamma_h}{\{\Gamma_h^2 + [E' - E_{j'}^h(\mathbf{k}_\parallel)]^2\} \{\Gamma_e^2 + [\hbar\omega - E_g - E' - E_j^e(\mathbf{k}_\parallel)]^2\}}, \end{aligned} \quad (17)$$

where $\hbar\omega$ is the photon energy, $E_g = 1.524 - 5.405 \times 10^{-4}T/(T+204)$ eV is the T -dependent energy gap of GaAs material, T is in kelvin, $E_1^{e,h}(k_y^{min})$ are the minimum ground-state energies of the electrons (e) and the holes (h), and $L_z = L_B + 2L_W$ is the total length of the active region in the DQW's. The quantities Γ_e and Γ_h are the homogeneous broadening of the electron and hole states. The line shape of the photoluminescence spectrum is a very complicated issue.^{24,25} In general, it depends on electron-impurity, electron-phonon, electron-interface roughness, and electron-electron scattering. Scattering mainly causes a finite lifetime for electrons and holes and the shift of band edges that are insensitive to the magnetic field. Here, we study the magnetic-field dependence of the PL peak energy position. Therefore, constant level broadening for electrons and holes is adequate for studying the magnetic-field dependence of the PL spectra. The quantity ϵ_b is the average dielectric constant of the system. The Boltzmann distribution $f_0^h[E_j^h(\mathbf{k}_\parallel)]$ for nondegenerate holes is

$$f_0^h[E_j^h(\mathbf{k}_\parallel)] = \exp\left[\frac{E_1^h(k_y^{min}) - E_j^h(\mathbf{k}_\parallel)}{k_B T}\right], \quad (18)$$

where the prefactor in Eq. (18), which can be determined by the hole density, is omitted. Therefore, we only get the relative strength of the peaks in the PL spectra. The dipole transition-matrix element is

$$\frac{|M_{j,j'}^{e,h}(k_y)|^2}{m_0} = \left(\frac{m_0}{m_W^e} - 1\right) \frac{E_g + \Delta_0}{2(E_g + 2\Delta_0/3)} E_g \mathcal{Q}_{j,j'}^{e,h}(k_y), \quad (19)$$

where the oscillator strength $\mathcal{Q}_{j,j'}^{e,h}(k_y)$ is given by

TABLE I. Band offsets and effective masses in units of the free-electron mass and band offsets for the electrons and holes in GaAs/Al_{0.3}Ga_{0.7}As DQW's, where $m_W^{h,\perp}$ and $m_B^{h,\perp}$ represent $m_h^*(z)$ in the QW's and barriers, respectively.

ΔE_c (eV)	ΔE_v (eV)	m_W^e	m_B^e	m_W^h	m_B^h	$m_W^{h,\perp}$	$m_B^{h,\perp}$
0.244	0.184	0.0665	0.0914	0.09	0.12	0.4535	0.4955

$$\mathcal{Q}_{j,j'}^{e,h}(k_y) = \left| \int_{-\infty}^{+\infty} dz \phi_{j,k_y}^e(z) \phi_{j',k_y}^h(z) \right|^2. \quad (20)$$

We include the z -dependent effective mass in the Schrodinger equations, Eqs. (1) and (12), for electrons and holes. There is another effect of z -dependent effective mass on the overlap of electron and hole wave functions.²⁶ However, this effect is expected to be very small when the electron and hole states are well confined due to the exponentially small penetration of wave function into the barrier regions. In our calculation, we study the PL spectra between the tunneling split electron and hole ground states, which are both well confined inside the well region. When the center barrier is very thin, the penetration is moderate. Even in this case, however, the effect of the z -dependent effective mass on the overlap integral of the electron and hole wave functions in Eq. (20) is small because the domain of the integration from this narrow region is small. The broadened step function $S(x)$ in Eq. (17) is given by

$$S(x) = \frac{1}{2} + \frac{1}{\pi} \tan^{-1}\left(\frac{x}{\sqrt{\Gamma_e \Gamma_h}}\right). \quad (21)$$

In Eq. (19), $\Delta_0 = 0.343$ eV is the spin-orbit splitting of GaAs material.

IV. NUMERICAL RESULTS AND THEIR DISCUSSIONS

A. Symmetric Double Quantum Wells

We first discuss the result for symmetric DQW's (sample A) with the following parameters: $\eta = 0.30$, $L_W = 100$ Å, $L_B = 35$ Å, $L_S = 50$ Å, and $N_D^L = N_D^R = 1.2 \times 10^{11}$ cm⁻². We approximate $\Gamma_e = \Gamma_h = \Gamma$ and assume that Γ is a constant for

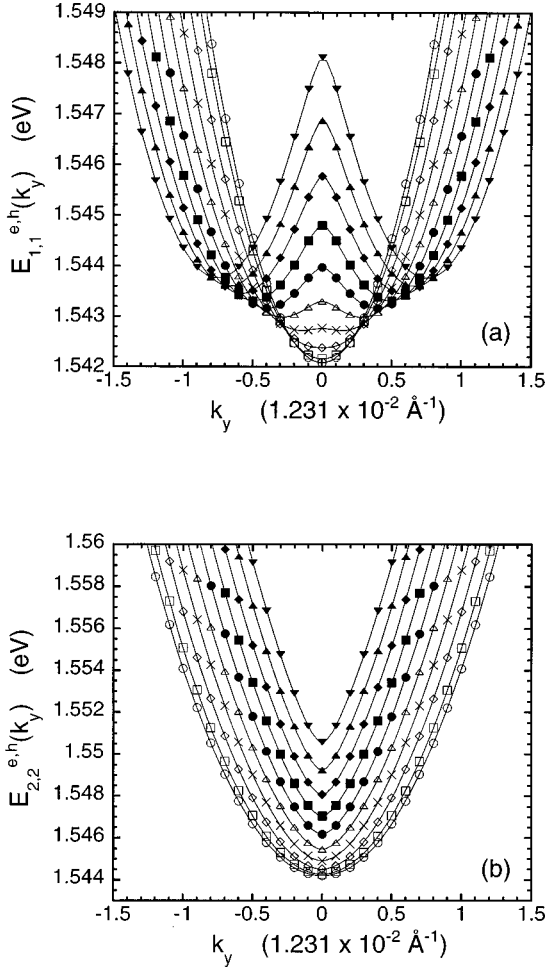


FIG. 3. Energy separations $E_j^e(k_y) + E_j^h(k_y)$ between (a) the lower ($j=1$) and (b) the upper ($j=2$) branches of the ground doublets of the electrons and holes of sample A as a function of k_y with various $B_{||}$ from 0 to 9 T. The curves with specific symbols from the bottom (\circ) to the top (\blacktriangledown) at $k_y=0$ correspond to $B_{||}=0$ to 9 T, in 1 T increments.

simplicity. Figures 3(a) and 3(b) present two groups of resonant photon energies $E_{j,j'}^{e,h}(k_y)$ for the momentum-conserving interband transitions, namely $E_j^e(k_y) + E_{j'}^h(k_y)$ as a function of k_y . The successive curves from the bottom to the top show $B_{||}$ -dependent behavior as $B_{||}$ is varied from 0 to 9 T. The curves in Fig. 3(a) represent the transitions between the lower branches ($j=j'=1$) of the tunnel-split ground doublets of the electrons and holes, while those in Fig. 3(b) arise from the transitions between the upper branches ($j=j'=2$). The interesting gradual development of the center peak at $k_y=0$ above $B_{||}=3$ T in Fig. 3(a) is due to the formation of the saddle point as the two minima move away from $k_y=0$ as discussed in the Introduction. In addition, there is an increase in energy for all k_y due to the diamagnetic shift.

When $B_{||} \neq 0$, the symmetry of the system is broken. As a result, the forbidden transitions $E_{1,2}^{e,h}(k_y)$ and $E_{2,1}^{e,h}(k_y)$ at $B_{||}=0$ become possible when $B_{||} \neq 0$, although they are relatively weak in strength compared to the transitions $E_{1,1}^{e,h}(k_y)$ and $E_{2,2}^{e,h}(k_y)$. The oscillator strength is proportional to $Q_{j,j'}^{e,h}(k_y)$, which is defined in Eq. (20). In Figs. 4(a) and

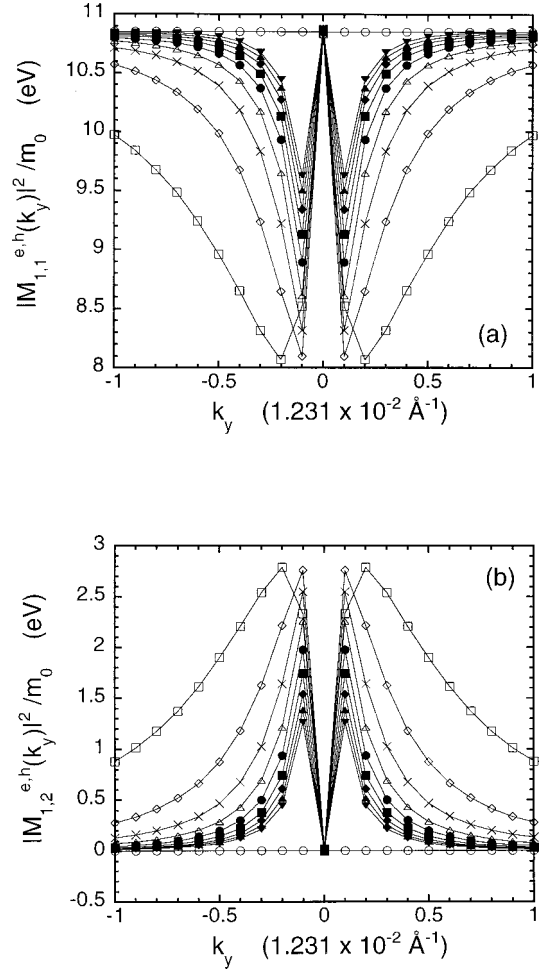


FIG. 4. Oscillator strengths $\propto Q_{j,j'}^{e,h}(k_y)$ for the transitions between the lower branch ($j=1$) of the electrons and (a) the lower ($j'=1$) and (b) the upper ($j'=2$) branches of the holes as a function of k_y for various $B_{||}$ from 0 to 9 T at 4 K. The symbol on each curve is the same as that used in Fig. 3.

4(b), we display $|M_{j,j'}^{e,h}(k_y)|^2/m_0 \propto Q_{j,j'}^{e,h}(k_y)$ for the transitions between the lower branch in the conduction band (i.e., $j=1$) and the lower ($j'=1$) and the upper ($j'=2$) branches in the valence band for various $B_{||}$'s. In the absence of the magnetic field (i.e., $B_{||}=0$), we have $Q_{j,j'}^{e,h}(k_y) = \delta_{jj'}$, namely, only the transitions between the states with the same parity are allowed for all k_y 's as shown by the empty circles in Fig. 4. With the application of $B_{||}$, however, only the states at $k_y=0$ preserve parity, yielding $Q_{j,j'}^{e,h}(0) = \delta_{jj'}$. For asymptotically large values of k_y , the separation between the unperturbed energy parabolas of the two QW's are very large, yielding negligible mixing (i.e., tunneling) between the two wells. For $k_y > 0$ ($k_y < 0$), the confinement wave functions $\phi_{1k_y}^e(z)$ and $\phi_{1k_y}^h(z)$ approach the wave function of the noninteracting right (left) well, while $\phi_{2k_y}^h(z)$ approaches that of the left (right) well. As a result, $Q_{1,1}^{e,h}(k_y)$ approaches unity and $Q_{1,2}^{e,h}(k_y)$ becomes small at large $|k_y|$ as shown in Fig. 4. For intermediate values of k_y , the quantity $Q_{1,j'}^{e,h}(k_y)$ has two minima for $j'=1$ and two maxima for $j'=2$. The extremum points move toward $k_y=0$ for increasing $B_{||}$ as

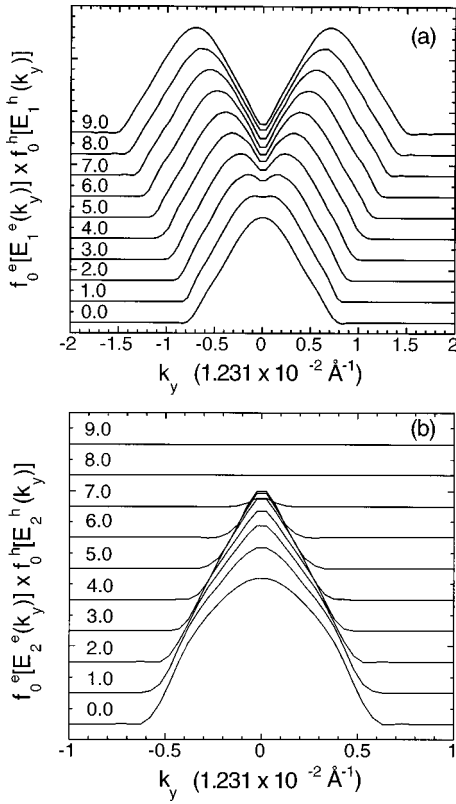


FIG. 5. Products of the electron and hole occupation functions for (a) the lower and (b) the upper branches of the ground doublets at 4 K, as a function of k_y for various B_{\parallel} from 0 to 9 T. The number on each curve represents B_{\parallel} value in tesla.

shown in Fig. 4, because the above discussed asymptotic behavior develops at smaller k_y values at higher B_{\parallel} 's due to a larger displacement Δk_y .

Figures 5(a) and 5(b) display the B_{\parallel} dependence of the product of the populations of electrons and holes in the ground doublets as a function of k_y for the transitions studied in Fig. 3. The minima at $k_y = 0$ in Fig. 5(a) above $B_{\parallel} \geq 2$ T are caused by the depopulation of the holes which was already illustrated in Fig. 1(b). At $B_{\parallel} = 9$ T, the electrons are also completely depopulated from the saddle point, because the saddle point has passed through the chemical potential. At this field, the hole population at $k_y = 0$ is still a few percent of the $B_{\parallel} = 0$ population due to thermal effects. The change in the product of the populations of electrons and holes in the lower branch is dominated by the holes at low fields and by the electrons at high fields. In Fig. 5(b) we find that the product of the populations of electrons and holes is zero at $B_{\parallel} = 8$ T because the chemical potential lies within the gap region. The gradual narrowing of the curves in Fig. 5(b) for increasing B_{\parallel} is due to the gradual depopulation of the upper branches, which starts in the large- $|k_y|$ regions and ends at $k_y = 0$. This depopulation is dominated by the holes at low fields and by the electrons at high fields.

Figure 6 shows the profiles of the single-particle (SP) conduction- and valence-band edges on the right axis, and their shifts due to the self-consistent Hartree (SCH) potential (dash-dotted lines) and the density-functional (DF) result (solid lines) on the left axes at $B_{\parallel} = 3$ T. The latter includes the exchange-correlation effect for the electrons and the cor-

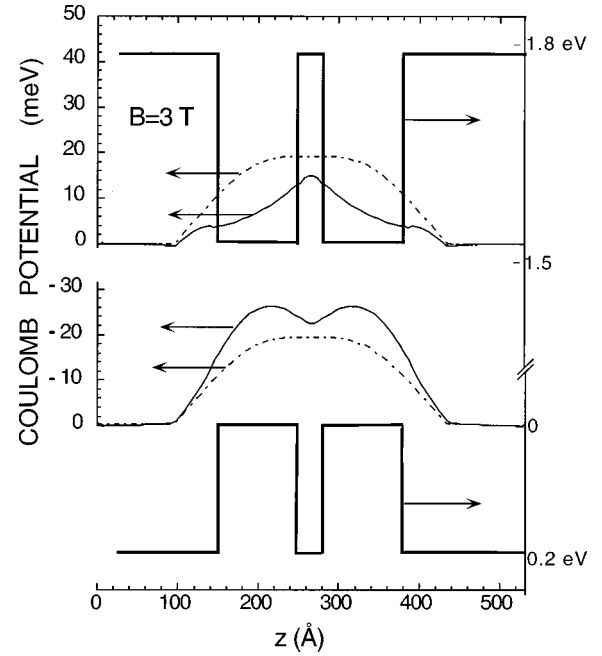


FIG. 6. Conduction- and valence-band edges (right axis) as well as the Coulomb potentials for the electrons and holes (left axis) in symmetric double quantum wells as a function of the distance z along the growth direction at $B_{\parallel} = 3$ T. The dash-dotted and solid lines represent the results calculated from the self-consistent Hartree theory and the density-functional theory at 4 K, respectively.

relation effect for the holes. Note that the left and right axes have very different scales. The SCH shift is identical in the conduction and valence bands, resulting in no visible shift for the PL energy. However, the exchange-correlation energy lowers the conduction-band edge and raises the valence-band edge relative to the SCH energies as shown by the solid lines in Fig. 6, yielding a band-gap narrowing and a considerable reduction of the PL energy. The energy lowering in the conduction band due to the exchange-correlation effect is more pronounced inside the QW's due to their higher electron densities, resulting in a peak for the DF energy inside the center barrier. The same effect, together with the fact that holes are more localized inside the QW's due to their heavy effective mass, yields a more pronounced dip for the DF energy in the valence band inside the center barrier as shown in Fig. 6. This peak-dip effect is more pronounced for a large B_{\parallel} where the electrons are more localized inside the QW's.

Calculated PL spectra are displayed in Fig. 7 for various B_{\parallel} 's from 0 to 9 T. The B_{\parallel} development of the two PL peaks is indicated by dotted and dashed lines U and L . It is clear that the upper peak (dotted line) disappears above 6 T due to the gradual depopulation of the holes from the upper branch around $k_y = 0$ as seen from Fig. 5. This B_{\parallel} -dependent behavior of the peak energy is plotted in Fig. 8. The upper peak shows an \mathcal{N} -type kink and merges with the lower peak. Early observed spectra¹⁵ with large linewidths did not resolve the upper and lower peaks clearly but showed a flat B_{\parallel} dependence of the peak below 5 T, consistent with the result in Fig. 8. More recent data with narrower linewidths show a two-peak behavior²⁷ similar to that shown in Figs. 7–9. The calculated peak energy rises rapidly (e.g., nearly quadratically) as a function of B_{\parallel} above 6 T in good agreement with

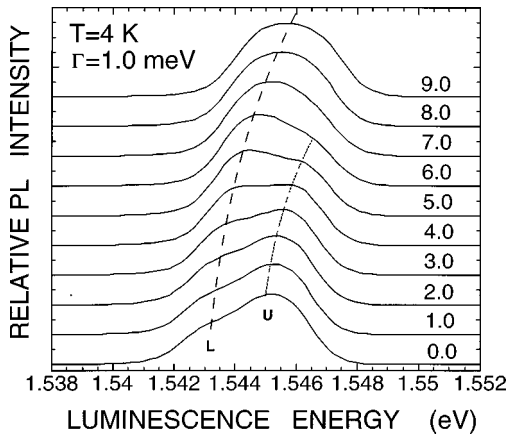


FIG. 7. Photoluminescence spectra at $T=4$ K for various B_{\parallel} from 0 to 9 T and $\Gamma=1.0$ meV. The dashed and dotted lines are guides to the eye for the lower and upper PL peaks.

the observed data.¹⁵ The B_{\parallel} -dependent evolution of the PL spectra is more clearly seen in Fig. 9 obtained for smaller damping $\Gamma=0.5$ meV. In this case, splitting of the two peaks is more clear, showing the abrupt switching of the strength from the high-energy peak to the low-energy peak at about $B_{\parallel}\sim 3$ T. At low B_{\parallel} 's near 0 T, the high-energy peak of the non-Lorentzian line shape appears much stronger than the low-energy peak because of the superposition of tail of the low-energy peak. The strength of the high-energy peak, however, diminishes rapidly at higher B_{\parallel} due to the depopulation of the carriers from the upper branch. The depopulation occurs first for the electrons in the upper branch for a system with a low-doping density. In a high-doping density system, the depopulation occurs first for the holes at $k_y=0$ at low temperatures.

Figures 10(a) and 10(b) display the comparison of the relative PL peak strengths of the upper and lower peaks [in (a)] and PL peak energies [in (b)] extracted from Fig. 9 as a function of B_{\parallel} from SP (dash-dotted line), SCH (dotted line), and DF (solid line) calculations. In Fig. 10(a), we find that the switching of the strength between the two PL peaks occurs around $B_{\parallel}=3$ T. The Coulomb interaction does not

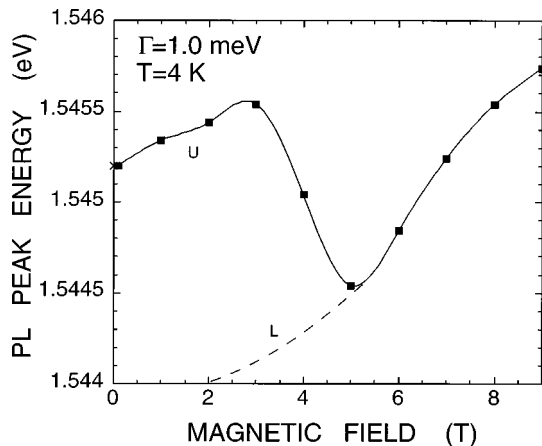


FIG. 8. Extracted PL peak energies from the calculated PL spectra in Fig. 7 as a function of B_{\parallel} . The solid square on the line represents the data from our calculation. The dashed line is the guide to the eye for the diamagnetic energy of the lower PL peak.

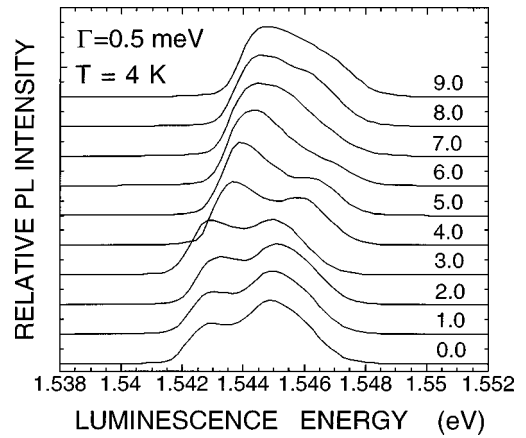


FIG. 9. Evolution of the PL spectra at 4 K for $\Gamma=0.5$ meV and for various B_{\parallel} from 0 to 9 T.

alter this switching feature in Fig. 10(a). It slightly reduces the strength of the high-energy PL peak as B_{\parallel} approaches to zero and that of the low-energy peak as B_{\parallel} becomes large. However, the exchange-correlation potential greatly reduces the PL peak energies by about 17 meV as shown in Fig. 10(b) by the solid curves. The reduction in the peak energies from the SP to the SCH approximations in Fig. 10(b) arises from the fact that the holes can maximize their energy lowering by situating themselves near the SCH potential minimum (see Fig. 6) without paying high confinement energy

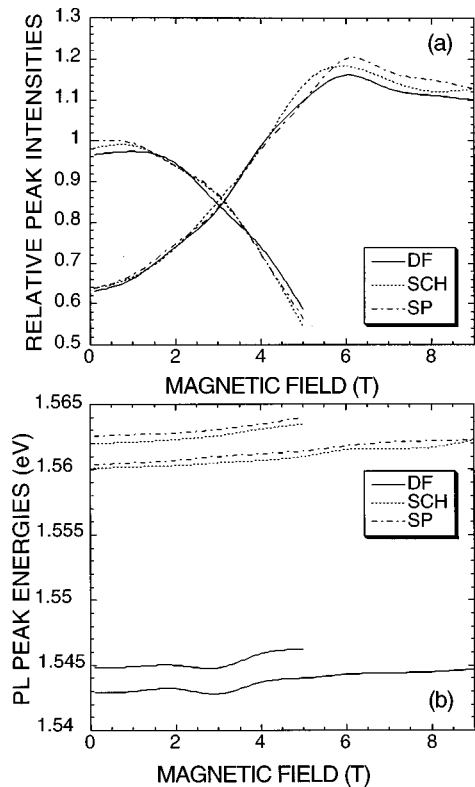


FIG. 10. Comparison of the relative PL peak strengths (a) and peak energies (b) in Fig. 9 as a function of B_{\parallel} calculated from the single-particle theory (dash-dotted line), self-consistent Hartree theory (dotted line), and the density-function theory (solid line). The peak due to PL from the saddle point is indicated with an arrow.

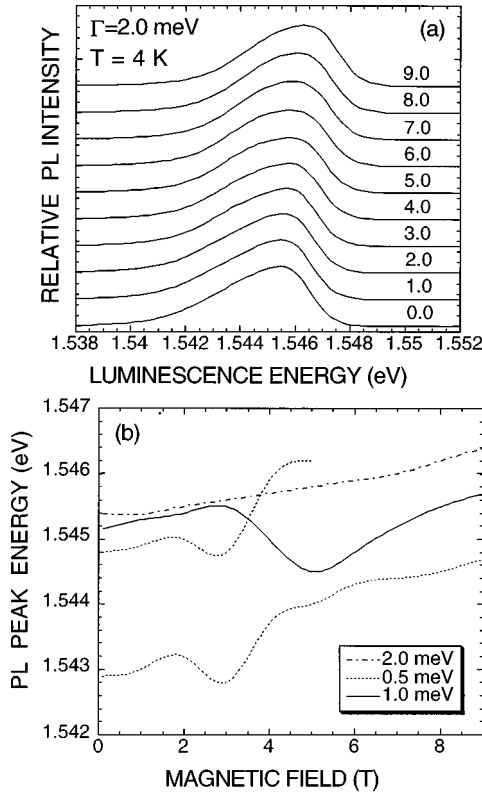


FIG. 11. (a) Evolution of the 4 K PL spectra with $\Gamma = 2.0$ meV for various B_{\parallel} from 0 to 9 T. (b) The peak energies as a function of B_{\parallel} for $\Gamma = 0.5$ meV (dotted line), $\Gamma = 1.0$ meV (solid lines), and $\Gamma = 2.0$ meV (dash-dotted line). For $\Gamma = 0.5$ meV, the upper (lower) curve is from the high- (low) energy PL peak.

because of their heavy confinement mass. As a result, the sublevels in the valence band move up in energy more than those in the conduction band, yielding the net reduction of the PL energy. Note that this SCH reduction is more pronounced for the upper peak than for the lower peak in Fig. 10(b). This is due to the SCH narrowing of the anticrossing gap in the conduction band. This narrowing arises from the fact that the electrons in the lower symmetric branch with relatively a large amplitude in the center barrier region feel a larger repulsive Hartree potential than the electrons in the upper asymmetric branch. The dips in Fig. 10(b) around $B_{\parallel} = 3$ T are the result of the competition between the enhancement of the band-gap narrowing due to the B_{\parallel} -induced localization of the carriers into the QW's and the diamagnetic energy. The latter dominates above $B_{\parallel} = 3$ T.

Figure 11(a) exhibits the PL spectra as a function of the energy with various B_{\parallel} from 0 to 9 T for a large homogeneous broadening $\Gamma = 2.0$ meV. Figure 11(b) displays the PL peak energies extracted from Figs. 9, 7, and 11(a) as a function of B_{\parallel} for $\Gamma = 0.5$, 1.0, and, 2.0 meV. From Fig. 11(a) we find that the doublet structure in the PL peak energies shown in Fig. 7, as well as the \mathcal{N} -type feature observed in Figs. 8, are completely smeared out by the large homogeneous broadening. From Fig. 11(b), we further see that the homogeneous broadening not only affects the line shape of the PL spectra, but also modifies the PL peak energies.

So far, we have discussed the PL at low temperatures. The main effect of high temperature is to thermally populate the holes near $k_y = 0$ and the electrons at the bottom of the upper

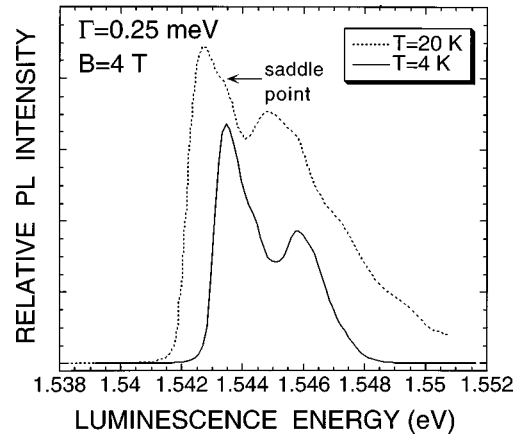


FIG. 12. PL spectra for $\Gamma = 0.25$ meV at 4 and 20 K at $B_{\parallel} = 4$ T.

branch even at high fields as illustrated in Fig. 1(c). As a consequence, the ratio of the strengths of the upper peak to that of the lower peak rises with the temperature. This effect is shown in Fig. 12, where the calculated PL spectra for $\Gamma = 0.25$ meV are plotted at 4 and 20 K at $B_{\parallel} = 4$ T. The effect of the thermal broadening and the T -dependent band narrowing is also seen clearly. The upper peak becomes stronger than the lower peak at $B_{\parallel} = 0$ T as in Fig. 9. At 20 K, there is an additional contribution to the PL from the electrons near the saddle point indicated by an arrow in Fig. 12 and illustrated in Fig. 1(c). The PL energy from the saddle point is close to the lower peak in Fig. 12 because the saddle point is barely formed at $B_{\parallel} = 4$ T. However, at a high field, the PL energy from the saddle point cannot be resolved from the upper peak, since the anticrossing gap is small (~ 2 meV).

B. Asymmetric Double Quantum Wells

When a dc electric field E_{dc} is applied to the symmetric DQW's, it changes into an asymmetric DQW because E_{dc} lifts both the conduction- and valence-band edges of the right QW compared to that of the left QW. Figure 13 presents the PL spectra of an asymmetric DQW for various magnetic fields in three different situations. The parameters chosen in our calculations are the same as those in sample A. We further choose $T = 4$ K and $\Gamma = 1.0$ meV and vary the doping densities.

In Fig. 13(a) we show the evolution of the PL spectra as a function of B_{\parallel} for medium doping densities $N_D^L = N_D^R = 1.2 \times 10^{11}$ cm $^{-2}$ and *high* dc field $E_{dc} = 10$ kV/cm. In this case, only the lower branches are populated for both the electrons and holes. The electrons are distributed in both QWs, while the holes occupy only the right QW for $0 \leq B_{\parallel} \leq 9$ T. The PL spectra show a wide-band emission with the low-energy and high-energy peaks prevailing, respectively, at low and high B_{\parallel} 's. This behavior can be understood from Fig. 2. At low B_{\parallel} 's, the dominant transitions are the low-energy transitions indicated by a dashed arrow in Fig. 2(a), since the upper branch is empty. These transitions are inter-QW transitions and are weak. At high B_{\parallel} 's, on the other hand, the dominant transitions are the high-energy transitions indicated by a solid arrow in Fig. 2(b). These transitions occur inside the right QW and yield a strong high-energy peak.

Figure 13(b) presents the evolution of the PL spectra with various B_{\parallel} 's for lower doping densities $N_D^L = N_D^R = 0.3$

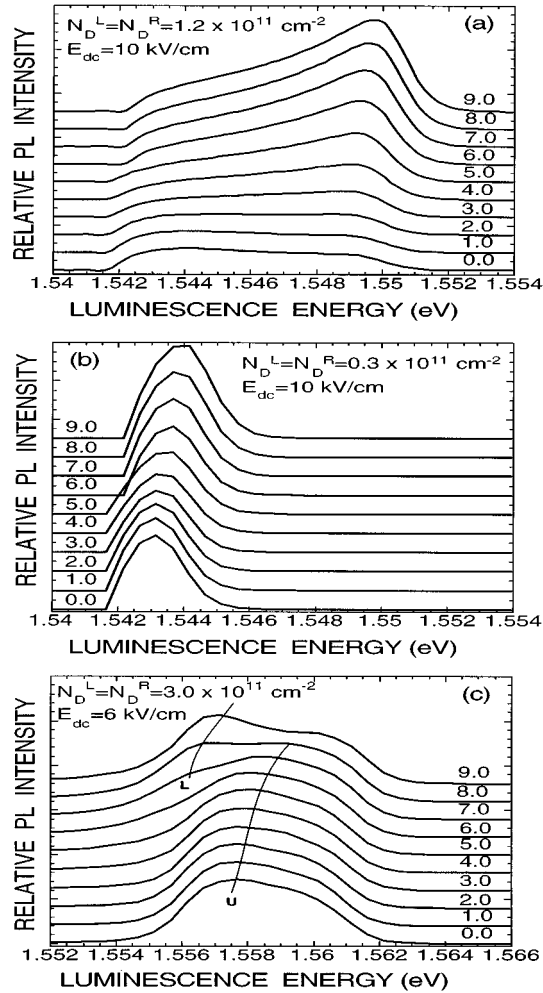


FIG. 13. Evolution of the 4 K PL spectra with $\Gamma = 1.0$ meV for various $B_{||}$ from 0 to 9 T for asymmetric DQW's. For (a) we have $N_D^L = N_D^R = 1.2 \times 10^{11} \text{ cm}^{-2}$ and $E_{dc} = 10$ kV/cm; For (b) we have $N_D^L = N_D^R = 0.3 \times 10^{11} \text{ cm}^{-2}$ and $E_{dc} = 10$ kV/cm; and for (c) we have $N_D^L = N_D^R = 3.0 \times 10^{11} \text{ cm}^{-2}$ and $E_{dc} = 6$ kV/cm. In (b) the scale for the intensity is about an order of magnitude smaller than in (a), while in (c) the scale is about an order of magnitude larger than in (a).

$\times 10^{11} \text{ cm}^{-2}$ and at the same dc field $E_{dc} = 10$ kV/cm. The basic difference between this low-density example and the above considered intermediate-density case is that the electrons are restricted within the left QW. The PL spectra show a narrow-peak emission, arising from weak low-energy interwell transitions only. Compared with Fig. 13(a), high-energy intrawell transitions have been completely suppressed in the whole range of $B_{||}$ considered here. The scale for the intensity is about an order of magnitude smaller in Fig. 13(b) than that in Fig. 13(a).

We display in Fig. 13(c) the evolution of the PL spectra as a function of $B_{||}$ for high-doping densities $N_D^L = N_D^R = 3.0 \times 10^{11} \text{ cm}^{-2}$ and low dc field $E_{dc} = 6$ kV/cm. In this case, the holes populate only the lower branch, while the electrons populate both the lower and upper branches. At low $B_{||}$'s, the strong peak in Fig. 13(c) arises from the intra-QW transitions from the upper branch shown by a solid arrow in Fig. 2(a). At high $B_{||}$'s, these transitions come from the upper edge of

the anticrossing gap as indicated by a shaded arrow in Fig. 2(b). The intensity of this high-energy peak decreases at higher $B_{||}$'s because the holes become less available. Note that these transitions between the upper electron branch and the lower hole branch are allowed by the asymmetry of the DQW's. At the same time, stronger intra-QW transitions indicated by a solid arrow in Fig. 2(b) split off, yielding a stronger PL peak at a somewhat lower energies as shown in Fig. 13(c). This behavior is similar to that shown by symmetric DQW's except that the lower PL peak is absent. Note that the scale for the intensity is about an order of magnitude larger in Fig. 13(c) than that in Fig. 13(a).

A single-to-double PL peak transition induced by $B_{||}$ was observed in a previous experiment²⁸ from undoped asymmetric DQW's with a wide QW and a narrow QW separated by a thin barrier. The electrons and holes, generated in the narrow QW, tunnel and relax quickly into the wide QW with lower ground sublevel energies at low temperatures. As a result, only the low-energy PL peak was observed from the wide QW at $B_{||} = 0$. At high $B_{||}$'s, however, the interwell tunneling is quenched, yielding an additional higher-energy PL peak from the narrow well. The transition here is of a dynamical origin and is very different from that of the present n -doped system, where the electrons reside in both QW's at a $B_{||}$'s.

V. CONCLUSIONS AND REMARKS

In this paper, we have demonstrated that the PL spectra from tunnel-split ground sublevels of DQW's are sensitively controlled by $B_{||}$ at low temperatures due to the $B_{||}$ -induced distortion of the electronic structure. With the density-functional theory, PL spectra with large band-gap narrowings have been found as a function of $B_{||}$, T , and Γ . In symmetric DQW's, two PL peaks have been obtained at $B_{||} = 0$, as a result of the interband transitions of the upper and lower branches of the ground doublets of the electrons and holes. When $B_{||}$ is increased, the upper PL peak develops an \mathcal{N} -type kink and merges with the lower peak at large $B_{||}$. At low-doping densities, however, the upper electron branch is empty, yielding only one PL peak. Asymmetric DQW's, created by applying a dc bias field, are also considered. In this case, the following three different types of $B_{||}$ -evolution of the PL spectra are obtained. (1) At a low-doping density where the electrons and holes are separated in the left and right QW's, respectively, the PL spectra show a single weak low-energy peak [see Fig. 13(b)] which arises from inter-QW transitions. (2) At an intermediate-doping density where the electrons are still only in the lower branch but are in both QW's, the PL peak shifts from the above low-energy peak at low $B_{||}$'s to a much stronger high-energy peak at high $B_{||}$'s [see Fig. 13(a)] arising from the intra-QW transitions in the right QW, indicated by a solid arrow in Fig. 2(b). (3) At a high doping density where the electrons populate both branches, a single peak with an \mathcal{N} -type kink behavior [see Fig. 13(c)], similar to that of symmetric DQW's, is obtained.

In our calculation, mixing of the heavy- and light-hole states is neglected due to small in-plane momentum of photo-excited hole states. The exchange-correlation is included in the density-functional theory, which is expected to lead to a relatively accurate result for the tunneling split elec-

tron and hole ground states at low temperatures. The effect of z -dependent effective masses of electrons and holes on the overlap of electron and hole wave functions is also neglected due to the strong confinement on the electron and hole ground-state wave functions. The effect of the scattering of electrons and holes by the impurities in the doping layers are included phenomenologically in Γ . We emphasize that the conclusions drawn in this paper will not be changed by the approximations used in our calculation. The impurity scattering is responsible for the complicated magnetic-field dependence of the spectral broadening.²⁷ This can alter the line shape of the PL peaks and can slightly shift the peak energies. A more complete theory, which includes the impurity

scattering in the self-consistent Born approximation is necessary for a more detailed comparison between the theory and experiment.

ACKNOWLEDGMENTS

One of the authors was supported by the United States Department of Energy under Contract No. DE-AC04-94AL85000 (S.K.L.). The authors thank Dr. Y. Kim of Los Alamos Laboratory and Dr. C. H. Perry of Northeastern University for sharing their data with them and for valuable discussions. The authors thank Dr. J. A. Simmons for a critical reading of the manuscript.

-
- ¹J. P. Eisenstein, T. J. Gramila, L. N. Pfeiffer, and K. W. West, *Phys. Rev. B* **44**, 6511 (1991).
- ²J. A. Simmons, S. K. Lyo, J. F. Klem, M. E. Sherwin, and J. R. Wendt, *Phys. Rev. B* **47**, 15 741 (1993).
- ³S. K. Lyo and J. A. Simmons, *J. Phys.: Condens. Matter* **5**, L299 (1993).
- ⁴L. Zheng and A. H. MacDonald, *Phys. Rev. B* **47**, 10 619 (1993).
- ⁵S. K. Lyo, *Phys. Rev. B* **50**, 4965 (1994).
- ⁶J. A. Simmons, S. K. Lyo, N. E. Harff, and J. F. Klem, *Phys. Rev. Lett.* **73**, 2256 (1994).
- ⁷A. Kurobe, I. M. Castleton, E. H. Linfield, M. P. Grimshaw, K. M. Brown, D. A. Ritchie, M. Pepper, and G. A. C. Jones, *Phys. Rev. B* **50**, 4889 (1994).
- ⁸O. E. Raichev and F. T. Vasko, *Phys. Rev. B* **53**, 1522 (1996).
- ⁹T. Jungwirth, T. S. Lay, L. Smrcka, and M. Shayegan, *Phys. Rev. B* **56**, 1029 (1997).
- ¹⁰N. E. Harff, J. A. Simmons, S. K. Lyo, J. F. Klem, G. S. Boebinger, L. N. Pfeiffer, and K. W. West, *Phys. Rev. B* **55**, R13 405 (1997).
- ¹¹M. Blount, J. A. Simmons, and S. K. Lyo, *Phys. Rev. B* **57**, 14 882 (1998).
- ¹²J. A. Simmons, N. E. Harff, and J. F. Klem, *Phys. Rev. B* **51**, 11 156 (1995).
- ¹³S. K. Lyo, *Phys. Rev. B* **51**, 11 160 (1995).
- ¹⁴I. S. Millard, N. K. Patel, C. Foden, E. H. Linfield, D. A. Ritchie, G. A. C. Jones, and M. Pepper, *J. Phys.: Condens. Matter* **9**, 1079 (1997).
- ¹⁵Y. Kim, C. H. Perry, D. G. Rickel, J. A. Simmons, J. F. Klem, and E. D. Jones, in *Proceedings of the 23rd International Conference on The Physics of Semiconductors*, edited by M. Scheffler and R. Zimmarmann (World Scientific, Singapore, 1996), p. 1859.
- ¹⁶S. Das Sarma, R. Jalabert, and S.-R. Eric Yang, *Phys. Rev. B* **41**, 8288 (1990).
- ¹⁷I. K. Marmorokos and S. Das Sarma, *Phys. Rev. B* **44**, 3451 (1991).
- ¹⁸L. Hedin and B. I. Lundqvist, *J. Phys. C* **4**, 2064 (1971).
- ¹⁹G. Platero and M. Altarelli, *Phys. Rev. B* **39**, 3758 (1989).
- ²⁰P. A. Bobbert, H. Wieldraaijer, R. van der Weide, M. Kemerink, P. M. Koenraad, and J. H. Wolter, *Phys. Rev. B* **56**, 3664 (1997).
- ²¹E. Enderlein, G. M. Sipahi, L. M. R. Scolfaro, and J. R. Leite, *Phys. Rev. Lett.* **79**, 3712 (1997).
- ²²S. K. Lyo and E. D. Jones, *Phys. Rev. B* **38**, 4113 (1988).
- ²³W. J. Fan, M. F. Li, and T. C. Chong, *J. Appl. Phys.* **80**, 3471 (1996).
- ²⁴O. E. Raichev and F. T. Vasko, *Phys. Rev. B* **50**, 5462 (1994).
- ²⁵O. E. Raichev and F. T. Vasko, *Phys. Rev. B* **51**, 7116 (1995).
- ²⁶R. Q. Yang, *Phys. Rev. B* **52**, 11 958 (1995).
- ²⁷Y. Kim *et al.* (unpublished).
- ²⁸M. L. Skorikov, I. I. Zasavitskiĭ, I. P. Kazakov, N. N. Sibel'din, V. A. Tsvetkov, and V. I. Tsekhosh, *Zh. Eksp. Fiz. Pis'ma Red.* **62**, 500 (1995) [*JETP Lett.* **62**, 522 (1995)].